Glyph-Based Uncertainty Visualization and Analysis of Time-Varying Vector Fields

Timbwaoga A. J. Ouermi *
SCI Institute, University of Utah

Jixian Li †
SCI Institute, University of Utah

Zachary Morrow ‡
Sandia National Laboratories

Bart van Bloemen Waanders §
Sandia National Laboratories

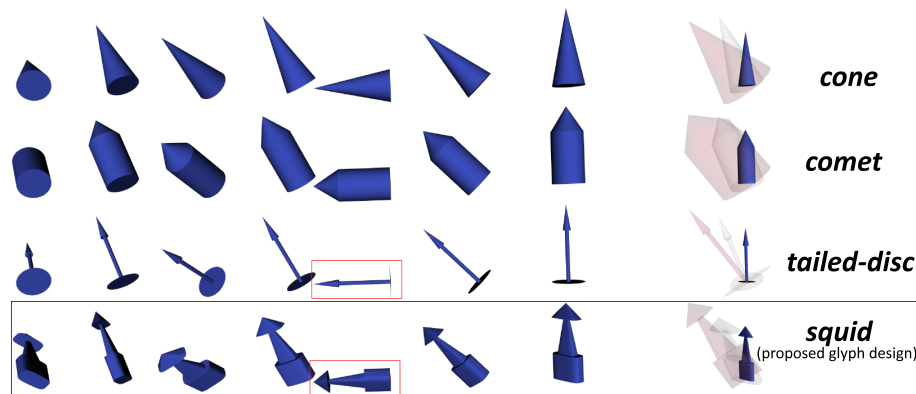Chris R. Johnson ¶
SCI Institute, University of Utah

Figure 1: 3D vector uncertainty glyph. The glyphs' direction corresponds to the median vector direction. The angle and length of the *cone* glyph represent the angular variation (the maximum angle between all pairs of vectors within the ensemble) and the maximum vector length. The magnitude variation (the difference between the maximum and minimum magnitude) is not included. The *comet* glyph encodes the magnitude variation and minimum magnitude using the length of the cone and cylinder, respectively. However, these variations are not easily discernible. While both the *tailed-disc* and *squid* clearly distinguish these uncertainties, the small arrow size and rotational symmetry of the *tailed-disc* limit the perception of the size of the uncertainty. In contrast, our proposed *squid* glyph effectively distinguishes between magnitude and direction variations. Additionally, it employs a superellipse (2D superquadric) to better approximate directional variations, eliminating rotational ambiguity around the median direction. The last column shows the uncertainty variation between the selected time step (opaque blue) and the next two time steps shown in transparent grey and red. The *squid* glyph is more accurate and less prone to rotational degeneracy.

ABSTRACT

Uncertainty is inherent to most data, including vector field data, yet it is often omitted in visualizations and representations. Effective uncertainty visualization can enhance the understanding and interpretability of vector field data. For instance, in the context of severe weather events such as hurricanes and wildfires, effective uncertainty visualization can provide crucial insights about fire spread or hurricane behavior and aid in resource management and risk mitigation. Glyphs are commonly used for representing vector uncertainty but are often limited to 2D. In this work, we present a glyph-based technique for accurately representing 3D vector uncertainty and a comprehensive framework for visualization, exploration, and analysis using our new glyphs. We employ hurricane and wildfire examples to demonstrate the efficacy of our glyph design and visualization tool in conveying vector field uncertainty.

Index Terms: time-dependent vector field uncertainty, data-depth, vector depth, vector field visualization, uncertainty glyph

*e-mail: touermi@sci.utah.edu

†e-mail: jixianli@sci.utah.edu

‡e-mail: zbmorro@sandia.gov

§e-mail: bartv@sandia.gov

¶e-mail: crj@sci.utah.edu

1 INTRODUCTION

Visualization and analysis of vector field data is fundamental to many scientific applications including flow simulations, weather prediction, and wildfire simulations. For example, in the context of wildfires, understanding wind uncertainty and flow patterns is critical for forecasting the overall fire behavior and ultimately providing more information to aid in resource management and risk mitigation. The wind data in these scenarios are inherently time-varying, three-dimensional, and associated with uncertainties.

Effective techniques for visualizing uncertainty in vector field data can improve understanding and interpretability [13, 25, 4]. Uncertainty visualization provides an understanding of the limitations and potential errors in the data, as well as insight into the observed features and trends in the vector field.

In this work, we present a glyph-based method for visualization and analysis of time-dependent 3D vector field uncertainty. Glyph-based methods for vector field uncertainty visualization have mostly been limited to 2D [20, 5, 29, 32, 7, 8, 27, 4, 6], and existing 3D glyph-based methods are prone to rotational ambiguity and do not provide insight into the distribution of vectors within the high uncertainty region. We address these limitations through the following contributions: (1) A 3D uncertainty glyph, we have named the *squid* glyph, that is designed using superellipses and cones to provide a more accurate approximation of the vector magnitude and direction uncertainty compared to the uncertainty *cone* [12], *comet* (cylinder + cone) [17], and *tailed-disc* (disc + arrow) [12] glyphs. Our *squid* glyph is suitable for representing anisotropy in directional variation and is less prone to visual ambiguity; (2) The use of

multivariate data depth, which we refer to as "vector depth" for exploration and analysis. The vector depth measures how immersed a given vector is compared to other vectors in a set. This metric provides insight into the distribution and individual vectors at each spatiotemporal location without prior assumptions about the distribution; and (3) A visualization framework that utilizes the *squid* glyph, the vector depth, and other methods to enable interactive visualization, exploration, and analysis of time-varying vector field uncertainty.

2 RELATED WORK

Several glyph-based methods have been developed to integrate uncertainty in order to improve understanding and interpretability of vector field visualization [29, 19, 21, 7, 8, 12, 31, 10, 32, 4]. Uncertainty in vector fields is often incorporated into the visualization as an add-on by overloading or modifying visual attributes such as surface reflectance, rendering opacity, and color to represent the uncertainty [3, 5, 19].

The work in [29, 30, 19] proposes different 2D glyph designs where the vector magnitude and angular variation are encoded in the length and shape of the glyph. Jarema et al. [8] propose a glyph-based methods that fits the vector field distribution at each location with the Gaussian mixture model (GMM) and a 2D lobular glyph overloaded with a colormap to visualize the distribution and uncertainty. Halwatsch et al. [7] proposed flow-radar glyphs for visualization of time-varying vector fields and their extension to incorporate magnitude and direction uncertainty in 2D. The flow-radar glyph is constructed by spatially and radially organizing the temporal vector direction into a sequence of points that are connected to form the glyph. Zuk et al. [32] utilize animation with 2D glyph representations to visualize the bidirectional vector field uncertainty in the context of analyzing anisotropy of rocks. Lee and Park [12] proposed a 3D glyph design to improve the representation of uncertainty and visual perception of the vector field data. This approach combines a disc and arrow glyph to encode the uncertainty. Schmidt et al. [21] use box, sphere, and cylinder glyphs to represent scalar uncertainty and arrow glyphs overloaded with color to represent directional uncertainty. Post et. al [20] proposed geometric primitives such as arrows and ellipses to encode and render 3D vectors and its distribution.

3 METHODS

Several uncertainties, including measurement, data transformation, and parameter variation, occur in 3D vector field. The instruments typically provide the uncertainty for measured data [28]. The uncertainties from data transformation and parameter variations can be estimated from ensemble data with statistical methods. Section 2 highlights different glyph-based methods for encoding the estimated uncertainties to different glyph attributes.

3.1 Uncertainty Glyph Design

The uncertainty glyph design is crucial for effectively visualizing the vector field uncertainty. We introduce the *squid* glyph, a 3D uncertainty glyph that builds on the ideas introduced in [29, 19] and leverages the design guidelines in [25, 13, 4]. Our *squid* glyph design primarily focuses on (1) accurately encoding the magnitude and direction uncertainty, (2) ensuring that the information encoded in the glyph is easily discernible, and (3) utilizing intuitive representations to provide insight into the vector field patterns and their uncertainties. We discuss these considerations sequentially. The design details of our *squid* glyph are illustrated in Fig. 2.

First, accurately mapping uncertainty information to glyph attributes is essential for the correct interpretation of individual uncertainty glyph and their relationships to neighboring glyphs. The use of ellipses can improve accuracy; however, it introduces a rotational degeneracy about the median direction of the glyph. In tensor
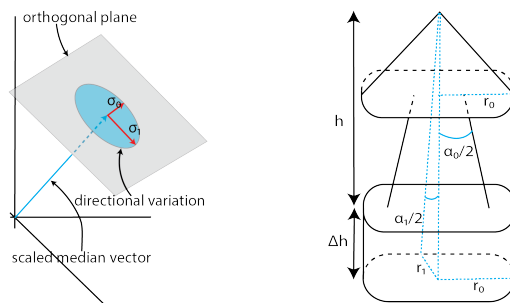

Figure 2: Uncertainty *squid* glyph design: The visualization on the left side illustrates calculating the first (σ_0) and second (σ_1) PCA principal components used to represent the directional spread and scale of the superellipse semi-minor axis. The diagram on the right side shows the *squid* glyph design with its parameters. The magnitude and magnitude variation are represented along the glyph direction. The minimum magnitude, magnitude variation, and maximum magnitude are represented with h, Δh, $h + \Delta h$, respectively.

visualization, superquadrics have been employed to enhance accuracy and remove rotational ambiguity [11, 22]. Following a similar approach, we utilize superellipses to design an uncertainty glyph that is both more accurate and less susceptible to rotational ambiguity. In Fig. 2, the minimum magnitude h, magnitude variation Δh, and the maximum magnitude $h + \Delta h$ are mapped to the length of the body, head, and entire glyph, respectively. The directional uncertainty is mapped to the angles α_0, α_1 and the semi-major axis r_0 and semi-minor axis r_1 of the superellipse at the base of the *squid* glyph shown on the right side of Fig. 2. The semi-major and semi-minor axis indicate the spread of the directional variation is calculated according to

$$r_0 = (h + \Delta h)\tan\left(\frac{1}{2}\alpha_0\right), \quad r_1 = r_0 \frac{||\sigma_1||}{||\sigma_0||}, \quad \alpha_1 = \tan^{-1}\left(\frac{h + \Delta h}{r_1}\right)$$

where α_0 is the maximum angle from the ensemble vectors at each spatiotemporal location. The visualization on the left side of Fig. 2 illustrates the process for calculating σ_0 and σ_1. They are obtained by finding the intersection of each vector with a plane orthogonal to the scaled median vector $(||v_{max}||/||v_{median}||)v_{median}$ and crosses its tip. The median vector v_{median} corresponds to the vector with the largest "vector depth" which is multivariate data depth that will be described in Sec. 3.2. We then employ principal component analysis (PCA) decomposition to find the first and second principal directions σ_0 and σ_1, respectively. The "squid" glyph direction corresponds to the median direction.

Second, individual glyph parts encoding the data information should be easily discernible. To facilitate interpretability, the glyph parts should be "orthogonal," meaning that each glyph part should be visually distinguishable independently [13]. To ensure orthogonality, our uncertainty *squid* glyph is designed such that the head, body, magnitudes, and angles can be perceived separately. These glyph attributes are normalized across the vector field data to enable comparison based on glyph sizes.

Lastly, given that arrows are a common and intuitive representation of directions and vectors, we utilize the cone and super-ellipse primitives to construct an arrow-like glyph that intuitively indicates size and direction. Glyphs that are designed based on semantic meaning are well-suited for interpretability and identifying features and patterns for visualization [25, 13, 4].

Occlusion and depth-perception limitations in 3D visualization impede the user's ability to effectively interpret spatial relationships and structures of the vector field and its uncertainty. We address this limitation by providing global and local interactive visualization ca-

pabilities that enable the user to focus on specific regions, or slices, thereby reducing occlusion and limitations of depth perceptions.

Figure 1 shows a comparison of our uncertainty *squid* glyph with the *comet*, *tailed-disc* [12], and the standard *cone* glyphs. The *cone* glyph only represents angular variation and not magnitude variations. The *comet* glyph does not clearly distinguish magnitude and direction variations. While both *tailed-disc* and *squid* glyphs depict these uncertainties, the *tailed-disc*'s small arrow size and rotational symmetry around the median direction limit the perception of the glyph's size, as highlighted in the orange boxes. In contrast, the *squid* glyph design effectively distinguishes between magnitude and direction variations. Additionally, it employs a superellipse to better approximate directional variations, eliminating rotational ambiguity around the median direction. Overall, the *squid* glyph is more accurate and less prone to rotational degeneracy.

3.2 Vector Depth

"Vector depth" is a multivariate data depth, a non-parametric statistical method for measuring centrality. It measures how deep or immersed a given vector is compared to other vectors in the dataset. The *squid* glyph in Sec. 3.1 provides a summary of the uncertainty at each spatiotemporal location, while the vector depth offers insights into the distribution of vectors from which the uncertainty summary is derived. The multivariate data depth approaches [15, 2, 14] have been extended to characterize contours [26], and curves [18]. Here, we adapt the multivariate data depth to vectors by computing the vector depth in spherical coordinates instead of standard Cartesian coordinates. Spherical coordinates are better suited for representing magnitude and direction variations.

Let F be a continuous probability distribution in $\Omega = \mathbb{R} \times [0, \pi] \times [-\pi, \pi]$, with $V = \{X_1, \ldots, X_n\} \subset \Omega$ a collection of $n > 3$ random samples from F. Any point in the 3D Cartesian coordinate ($\mathbb{R}^3$) can be uniquely represented in the spherical coordinate (Ω). The vector depth of x is the percentage of size-4 subsets of V whose bounding box in Ω contains x. Mathematically,

$$VD(x) = \binom{n}{4}^{-1} \sum_{\tilde{V} \subset V, |\tilde{V}|=4} \mathbf{1}_{S[\tilde{V}]}(x). \quad (1)$$

$S[\tilde{V}]$ is the closed region in spherical space with corners defined by $\tilde{V}$, and $\mathbf{1}$ is the indicator function (1 if $x \in S[\tilde{V}]$, 0 otherwise).

The data depth is suitable for identifying outliers and providing insight into vector distribution. Figure 3 shows a skewed distribution with an outlier on the left side, a *squid* glyph approximation of the distribution in the center, and a *squid* approximation without the outlier that is removed by excluding the smallest vector.

Figure 3: The arrows on the left side show the explicit visualization of the vector distribution. The *squid* glyph approximation for this distribution is shown in the center. The *squid* glyph representation without the outlier is shown on the left side.

3.3 Vector Field Uncertainty Visualization Tool

We present a visualization tool for the exploration and analysis of time-varying vector field data. Vector field uncertainties are often omitted, and when included, they are typically limited to 2D representations. Our framework leverages color, transparency, multiple views, the *squid* glyph, and "vector depth" of the previous two sections to enable a comprehensive global and local spatiotemporal analysis of vector-field uncertainty. The interface is designed

to highlight and provide insights into regimes with significant uncertainty while preserving the overall visual patterns of the vector field.

We employ an example dataset constructed by sampling the vector field in Eq. (2) and adding uniform random noise to each vector component. Specifically, the generated dataset includes 20 ensemble members at each spatiotemporal location, obtained by perturbing each vector component with uniform noise.

$$\begin{matrix} u_0 = \sin(x) \\ v_0 = \sin(y) \\ w_0 = 0.5 \end{matrix} \quad \begin{bmatrix} u_{t+1} \\ v_{t+1} \\ w_{t+1} \end{bmatrix} = \begin{bmatrix} u_t \cos(t) - v_t \sin(t) \\ u_t \sin(t) + v_t \cos(t) \\ w_t \end{bmatrix} \quad \begin{matrix} x \in [-1, 1] \\ y \in [-1, 1] \\ t \in [0, \frac{3}{4}\pi]. \end{matrix} \quad (2)$$

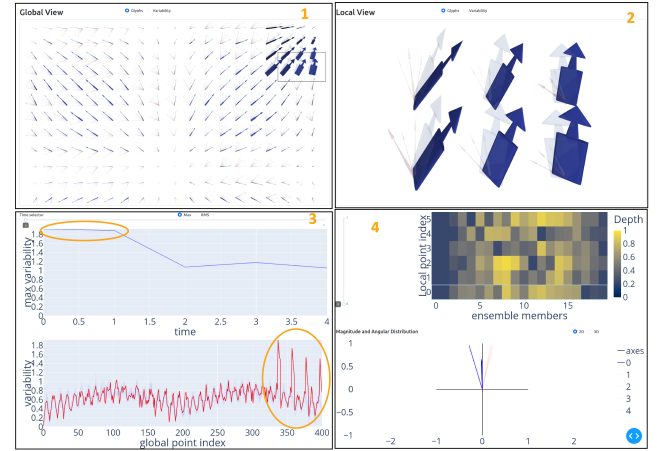Figure 4 shows the framework interface with the components in black rectangles and the numbers in orange.

Figure 4: Vector uncertainty analysis interface. The outlined black rectangles and orange numbers indicate the components. C_1 and C_2 are used for global and local visualization of filtered vector data, respectively. C_3 visualizes the magnitude variations and while C_4 visualizes the vector depth distribution magnitudes and angular variations at a selected location.

The component C_1 (top left) uses the *squid* glyph to show a global visualization of the vector field data while the second component C_2 (top right) shows a local visualization based on the selected region indicated by the black box in C_1. The component C_3 (bottom left) enables the visualization of magnitude variations for the specific a time range and specific selected time. The top plots in C_3 of Fig. 4 show the maximum magnitude variations (on the y-axis) versus time (x-axis) and the bottom plot shows the magnitude variations at each location for a selected time step. Both visualizations can help the user identify regions with large variations as shown with orange ellipses. The component C_4 visualizes the vector depth values and provides insight about the distribution of vectors at a selected spatiotemporal point. The top figure in C_4 uses heatmap visualization where the y-axis represents the spacial locations, the x-axis represents the ensemble members, and the colormap represents vector depth for the vectors in the C_2 at a selected time step. The bottom figure provides detailed information about the distribution of vectors from which the vector uncertainty is computed. The angular variation is calculated with respect to the median vector direction. These visualizations provide detailed information about the vector field uncertainty and can be employed to detect outliers, as shown in the bottom plot in C_4.

The variations are computed with respect to the data to provide an intuitive visualization and uncertainty analysis at the measured or sampled spatiotemporal locations directly. These computed variations can be used to guide measurement and resampling offline

(a) *comet* (hurricane)   (b) *tailed-disc* (hurricane)   (c) *squid* (hurricane)   (d) *comet* (wildfire)   (e) *tailed-disc* (wildfire)   (f) *squid* (wildfire)
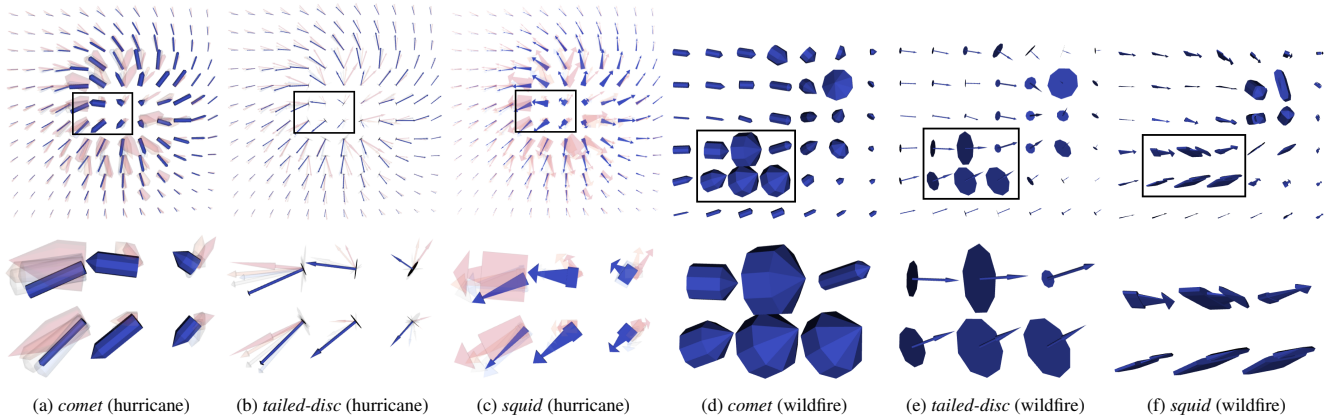
Figure 5: Hurricane Isabel and wildfire examples. Both examples show a comparison of the *comet*, *tailed-disc* and *squid* glyphs

to reduce uncertainty and improve data quality. In future studies, we plan to investigate Combining spatial, temporal, and parameter-based uncertainty altogether to provide additional insight and further enhance the uncertainty analysis.

4 RESULTS AND DISCUSSION

4.1 Hurricane Isabel

Hurricane Isabel was the most costly hurricane of the 2003 season with $3.6 billion in damage. In the context of hurricanes, understanding wind patterns and uncertainty is crucial for a better characterization of the hurricane behavior and to provide useful information that can aid in resource management and risk mitigation. The visualization dataset is obtained by down-sampling the original dataset [9] volume resolution from $500 \times 500 \times 100 \times 48$ to $40 \times 40 \times 100 \times 48$. The vector uncertainty at each sub-sampled location is obtained using the local neighborhood vectors in the $5 \times 5 \times 1$ spatial patch.

Figure 5a - Figure 5c show a comparison of the different glyph representations around the hurricane eye for a horizontal slice. The larger-size *comet* glyphs in Fig. 5a better highlight the regions with large uncertainty compared to the other approaches. However, the *comet* glyphs in Fig. 5a do not effectively differentiate between magnitude and directional variations. In contrast, these variations are distinguished in *tailed-disc* glyphs shown in Fig. 5b, but the *tailed-disc* design is not suitable for highlighting regions with large uncertainties. Figure 5c show that the proposed *squid* glyph design is suitable for (1) identifying regions with larger uncertainties, (2) distinguishing the magnitude and directional variation in each glyph, and (3) more accurately encoding the directional uncertainty dispersion compared the other approaches. The zoomed-in region enables uncertainty comparison of the currently selected time step with neighboring time steps indicated by using transparency and different colors. These results demonstrate that the *squid* glyph provides a more accurate representation of the vector uncertainties compared to the *comet* and *tailed-disc*.

4.2 Wildfire

This example models wildfire-produced winds resulting from uncertain fuel properties in the Valles Caldera National Preserve of northern New Mexico. This location was selected for its varied topography, well-defined fuel regions, and history of fire activity. There are three easily identifiable fuel regions: the caldera floor, forest edge, and forest. In reality, fuels are strongly dependent on fine-grained local properties, but state-of-the-art models treat them as bulk quantities for computational tractability, resulting in epistemic uncertainty. Moreover, material parameters in fire codes are typically set to *a priori* nominal values based on standard fuel models, e.g. [1, 23], resulting in aleatoric uncertainty.

For each of the three fuel regions, we sample the surface-area-to-volume ratio (SAVR) from a uniform distribution centered on the nominal parameter value. Using the state-of-the-art code WRF-SFIRE [16], we run a fire simulation for each SAVR sample, lasting $t = 10$ hours. The quantity of interest is the final-time, three-dimensional wind, defined on a 69×53 grid where $\Delta x = \Delta y = 150$m. The winds are initialized modestly at 1 m/s for dynamical stability, and topographic data comes from LANDFIRE [24].

Figure 5d - Figure 5f show a comparison of the different glyph designs applied to wildfire winds. The results in the zoomed-in region show that all four glyphs effectively highlight the region with large uncertainty shown in the black box. The magnitude and directional variations are more distinguishable in both the *tailed-disc* and *squid* glyphs, compared to the *comet* glyphs where the different parts are not easily discernible. Moreover, the *squid* glyph provides a more accurate representation and superior visualization of wind uncertainty. Additionally, the *squid* glyph provides a more accurate representation of the directional variations compared to the other methods that assume symmetry in the directional spread around the median direction. This provides insights into overall wind patterns and their associated variations due to changes in fuel content, thereby enhancing understanding of wildfire behavior.

5 CONCLUSION

In this paper, we introduced the *squid* glyph, a 3D vector field uncertainty glyph that accurately represents magnitude and direction uncertainties and is less prone to rotational ambiguity. In addition, we presented a visualization tool that utilizes the *squid* glyph, vector depth, and other techniques for exploration and analysis of vector field uncertainty. The *squid* glyph with pointy tip is suboptimal in cases with extensive angular variation. In the future, we plan to investigate the use of tensor glyphs and alternative design strategies, such as arrowheads with less accentuated shapes like half-ellipses to represent vector ensembles with multiple modes and wide variations to further enhance glyph design.

REFERENCES

[1] H. E. Anderson. Aids to determining fuel models for estimating fire behavior, 1982. Gen. Tech. Rep. INT-GTR-122. doi: 10.2737/int-gtr-122 4

[2] V. Barnett. The ordering of multivariate data. *Journal of the Royal Statistical Society. Series A (General)*, 139(3):318–355, 1976. 3

[3] G.-P. Bonneau, H.-C. Hege, C. R. Johnson, M. M. Oliveira, K. Potter, P. Rheingans, and T. Schultz. *Overview and State-of-the-Art of Uncertainty Visualization*, pp. 3–27. Springer London, London, 2014. doi: 10.1007/978-1-4471-6497-5_1 2

[4] R. Borgo, J. Kehrer, D. H. S. Chung, E. Maguire, R. S. Laramee, H. Hauser, M. Ward, and M. Chen. Glyph-based Visualization: Foundations, Design Guidelines, Techniques and Applications. In M. Sbert and L. Szirmay-Kalos, eds., *Eurographics 2013 - State of the Art Reports*. The Eurographics Association, 2013. doi: 10.2312/conf/EG2013/stars/039-063 1, 2

[5] E. Boring and A. Pang. Directional flow visualization of vector fields. In *Proceedings of Seventh Annual IEEE Visualization '96*, pp. 389–392, 1996. doi: 10.1109/VISUAL.1996.568139 1, 2

[6] D. H. Chung, R. S. Laramee, J. Kehrer, and H. Hauser. *Glyph-Based Multi-field Visualization*, pp. 129–137. Springer London, London, 2014. doi: 10.1007/978-1-4471-6497-5_13 1

[7] M. Hlawatsch, P. Leube, W. Nowak, and D. Weiskopf. Flow radar glyphs—static visualization of unsteady flow with uncertainty. *IEEE Transactions on Visualization and Computer Graphics*, 17(12):1949–1958, 2011. doi: 10.1109/TVCG.2011.203 1, 2

[8] M. Jarema, I. Demir, J. Kehrer, and R. Westermann. Comparative visual analysis of vector field ensembles. In *2015 IEEE Conference on Visual Analytics Science and Technology (VAST)*, pp. 81–88, 2015. doi: 10.1109/VAST.2015.7347634 1, 2

[9] M. Jiang, N. Shareef, C. Zhang, R. Crawfis, R. Machiraju, and H.-W. Shen. Visualization fusion: Hurricane isabel dataset. In *Proc. 15th IEEE Visualization Conf.(VIS'04), contest entry*, 2004. 4

[10] C. Johnson and A. Sanderson. A next step: Visualizing errors and uncertainty. *IEEE Computer Graphics and Applications*, 23(5):6–10, 2003. doi: 10.1109/MCG.2003.1231171 2

[11] G. Kindlmann. Superquadric tensor glyphs. In *Proceedings of the Sixth Joint Eurographics - IEEE TCVG Conference on Visualization*, VISSYM'04, p. 147–154. Eurographics Association, Goslar, DEU, 2004. 2

[12] J.-Y. Lee and J. Park. Perception-Aware Uncertainty Glyphs in the 3D Vector Fields. In J. Johansson, F. Sadlo, and T. Schreck, eds., *EuroVis 2018 - Short Papers*. The Eurographics Association, 2018. doi: 10.2312/eurovisshort.20181069 1, 2, 3

[13] A. E. Lie, J. Kehrer, and H. Hauser. Critical design and realization aspects of glyph-based 3d data visualization. In *Proceedings of the 25th Spring Conference on Computer Graphics*, SCCG '09, p. 19–26. Association for Computing Machinery, New York, NY, USA, 2009. doi: 10.1145/1980462.1980470 1, 2

[14] R. Y. Liu. On a notion of simplicial depth. *Proceedings of the National Academy of Sciences*, 85(6):1732–1734, 1988. doi: 10.1073/pnas.85.6.1732 3

[15] R. Y. Liu, J. M. Parelius, and K. Singh. Multivariate analysis by data depth: descriptive statistics, graphics and inference, (with discussion and a rejoinder by Liu and Singh). *The Annals of Statistics*, 27(3):783–858, 1999. doi: 10.1214/aos/1018031260 3

[16] J. Mandel, S. Amram, J. D. Beezley, G. Kelman, A. K. Kochanski, V. Y. Kondratenko, B. H. Lynn, B. Regev, and M. Vejmelka. Recent advances and applications of WRF-SFIRE. *Natural Hazards and Earth System Sciences*, 14(10):2829–2845, 2014. doi: 10.5194/nhess-14-2829-2014 4

[17] E. McQuinn, A. Chourasia, J. P. Schulze, and J.-B. Minster. GlyphSea: Visualizing Vector Fields. In P. C. Wong, D. L. Kao, M. C. Hao, and C. Chen, eds., *Visualization and Data Analysis 2014*, vol. 9017, p. 90170L. International Society for Optics and Photonics, SPIE, 2014. doi: 10.1117/12.2041248 1

[18] M. Mirzargar, R. T. Whitaker, and R. M. Kirby. Curve boxplot: Generalization of boxplot for ensembles of curves. *IEEE Transactions on Visualization and Computer Graphics*, 20(12):2654–2663, 2014. doi: 10.1109/TVCG.2014.2346455 3

[19] A. T. Pang, C. M. Wittenbrink, S. K. Lodha, et al. Approaches to uncertainty visualization. *The Visual Computer*, 13(8):370–390, 1997. 2

[20] F. Post, T. van Walsum, F. Post, and D. Silver. Iconic techniques for feature visualization. In *Proceedings Visualization '95*, pp. 288–295, 1995. doi: 10.1109/VISUAL.1995.485141 1, 2

[21] G. Schmidt, S.-L. Chen, A. Bryden, M. Livingston, L. Rosenblum, and B. Osborn. Multidimensional visual representations for underwater environmental uncertainty. *IEEE Computer Graphics and Applications*, 24(5):56–65, 2004. doi: 10.1109/MCG.2004.35 2

[22] T. Schultz and G. L. Kindlmann. Superquadric glyphs for symmetric second-order tensors. *IEEE Transactions on Visualization and Computer Graphics*, 16(6):1595–1604, 2010. doi: 10.1109/TVCG.2010.199 2

[23] J. H. Scott and R. E. Burgan. Standard fire behavior fuel models: A comprehensive set for use with Rothermel's surface fire spread model, 2005. Gen. Tech. Rep. RMRS-GTR-153. doi: 10.2737/rmrs-gtr-153 4

[24] U.S. Department of the Interior, Geological Survey, and Department of Agriculture. Landfire, 2023. Layers: Topographic Elevation. 4

[25] M. O. Ward. *Multivariate Data Glyphs: Principles and Practice*, pp. 179–198. Springer Berlin Heidelberg, Berlin, Heidelberg, 2008. doi: 10.1007/978-3-540-33037-0_8 1, 2

[26] R. T. Whitaker, M. Mirzargar, and R. M. Kirby. Contour boxplots: A method for characterizing uncertainty in feature sets from simulation ensembles. *IEEE Transactions on Visualization and Computer Graphics*, 19(12):2713–2722, 2013. doi: 10.1109/TVCG.2013.143 3

[27] A. Wiebel, S. Koch, and G. Scheuermann. *Glyphs for Non-Linear Vector Field Singularities*, pp. 177–190. Springer Berlin Heidelberg, Berlin, Heidelberg, 2012. doi: 10.1007/978-3-642-23175-9_12 1

[28] J. M. Wilczak, R. G. Strauch, F. M. Ralph, B. L. Weber, D. A. Merritt, J. R. Jordan, D. E. Wolfe, L. K. Lewis, D. B. Wuertz, J. E. Gaynor, S. A. McLaughlin, R. R. Rogers, A. C. Riddle, and T. S. Dye. Contamination of wind profiler data by migrating birds: Characteristics of corrupted data and potential solutions. *Journal of Atmospheric and Oceanic Technology*, 12(3):449 – 467, 1995. doi: 10.1175/1520-0426(1995)012<0449:COWPDB>2.0.CO;2 2

[29] C. Wittenbrink, A. Pang, and S. Lodha. Glyphs for visualizing uncertainty in vector fields. *IEEE Transactions on Visualization and Computer Graphics*, 2(3):266–279, 1996. doi: 10.1109/2945.537309 1, 2

[30] C. M. Wittenbrink, E. Saxon, J. J. Furman, A. Pang, and S. K. Lodha. Glyphs for visualizing uncertainty in environmental vector fields. In R. N. Ellson, G. G. Grinstein, and R. F. Erbacher, eds., *Visual Data Exploration and Analysis II*, vol. 2410, pp. 87 – 100. International Society for Optics and Photonics, SPIE, 1995. doi: 10.1117/12.205940 2

[31] T. Zuk and S. Carpendale. Theoretical analysis of uncertainty visualizations. In R. F. Erbacher, J. C. Roberts, M. T. Gröhn, and K. Börner, eds., *Visualization and Data Analysis 2006*, vol. 6060, p. 606007. International Society for Optics and Photonics, SPIE, 2006. doi: 10.1117/12.643631 2

[32] T. Zuk, J. Downton, D. Gray, S. Carpendale, and J. Liang. Exploration of uncertainty in bidirectional vector fields. In K. Börner, M. T. Gröhn, J. Park, and J. C. Roberts, eds., *Visualization and Data Analysis 2008*, vol. 6809, p. 68090B. International Society for Optics and Photonics, SPIE, 2008. doi: 10.1117/12.768317 1, 2